Inorganic Chemistry

Article

pubs.acs.org/IC

Synthesis and Structure of Trinuclear W_3S_4 Clusters Bearing Aminophosphine Ligands and Their Reactivity toward Halides and Pseudohalides

Tomás F. Beltrán,[†,§] Jose Ángel Pino-Chamorro,[‡,§] M. Jesús Fernández-Trujillo,[‡] Vicent S. Safont,*[,†] Manuel G. Basallote,*[,‡] and Rosa Llusar*[,†]

[†]Departament de Química Física i Analítica, Universitat Jaume I, Av. Sos Baynat s/n, 12071 Castelló, Spain

[‡]Departamento de Ciencia de los Materiales e Ingeniería Metalúrgica y Química Inorgánica, Facultad de Ciencias, Universidad de Cádiz, Apartado 40, Puerto Real, 11510 Cádiz, Spain

Supporting Information

ABSTRACT: The aminophosphine ligand (2-aminoethyl)-diphenylphosphine (edpp) has been coordinated to the $W_3(\mu\text{-}S)(\mu\text{-}S)_3$ cluster unit to afford trimetallic complex $[W_3S_4Br_3(edpp)_3]^+$ ($\mathbf{1}^+$) in a one-step synthesis process with high yields. Related $[W_3S_4X_3(edpp)_3]^+$ clusters (X = F^-, Cl^-, NCS^-; $\mathbf{2}^+$–$\mathbf{4}^+$) have been isolated by treating $\mathbf{1}^+$ with the corresponding halide or pseudohalide salt. The structure of complexes $\mathbf{1}^+$ to $\mathbf{4}^+$ contains an incomplete W_3S_4 cubane-type cluster unit, and only one of the possible isomers is formed: the one with the phosphorus atoms trans to the capping sulfur and the amino groups trans to the bridging sulphurs. The remaining coordination position on each metal is occupied by X. Detailed studies using stopped-flow, $^{31}P\{^1H\}$ NMR, and ESI-MS have been carried out in order to understand the solution behavior and the kinetics of interconversion among species $\mathbf{1}^+$, $\mathbf{2}^+$, $\mathbf{3}^+$, and $\mathbf{4}^+$ in solution. Density functional theory (DFT) calculations have been also carried out on the reactions of cluster $\mathbf{1}^+$ with the different anions. The whole set of experimental and theoretical data indicate that the actual mechanism of substitutions in these clusters is strongly dependent on the nature of the leaving and entering anions. The interaction between an entering F^- and the amino group coordinated to the adjacent metal have also been found to be especially relevant to the kinetics of these reactions.

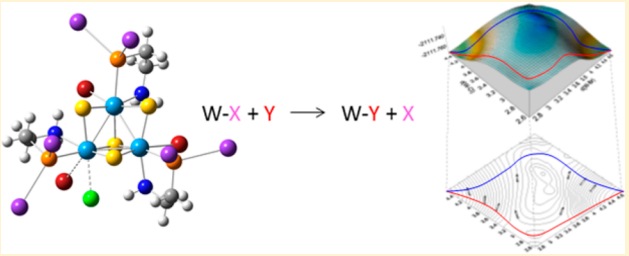

INTRODUCTION

Multifunctional catalysis, in which metal–metal and metal–ligand interactions cooperate to chemically transform a substrate as natural enzymes do, is currently a field of central interest.[1] In this context, cuboidal cluster chalcogenides (M_3S_4, M = Mo, W), represented in Figure 1, and their closely related heterobimetallic complexes ($M_3M'S_4$, M′ = transition metal) have been extensively investigated.[2] In general, molybdenum and tungsten M_3S_4 clusters are electron precise, with six electrons for the formation of the three metal–metal bonds and a formal oxidation state of +4 for the metals (Mo or W).

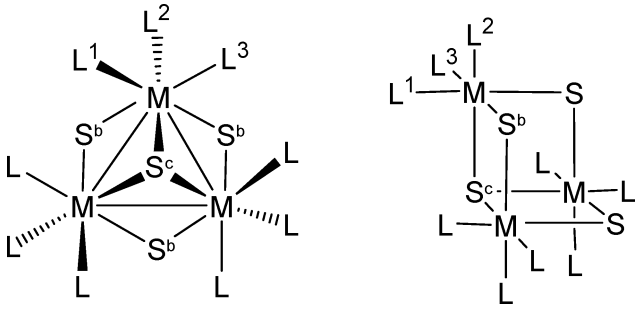

Figure 1. Two alternative views of the cuboidal $M_3S_4L_9$ cluster, showing the capping (S^c) and bridging (S^b) sulfur atoms. M–M bonds are omitted for clarity on the right side.

Particular attention has been paid in our groups to the diphosphino $[M_3S_4X_3(diphosphine)_3]^+$ derivatives (X = halide or hydride) because of the major role that transition-metal complexes containing phosphines play in homogeneous catalysis.[3−11] The coordination mode of the diphosphine ligands in these complexes affords a single isomer, represented in Figure 2, with one phosphorus atom trans to the capping sulfur (S^c) and one trans to the bridging sulfur (S^b), resulting in quiral clusters with C_3 symmetry. All three metals share an identical coordination environment. In the last several years, aminophosphines have emerged as versatile ligands because they combine the π-acceptor character of the phosphorus atom with the σ-donor properties of nitrogen.[12−14] In addition, the NH moieties from the aminophosphine that is directly coordinated to the metal center can take part in the catalytic reaction by cooperation with the metal-bonded species.[1] Thus, several

Received: October 17, 2014
Published: December 31, 2014

DOI: 10.1021/ic5025313
Inorg. Chem. 2015, 54, 607–618

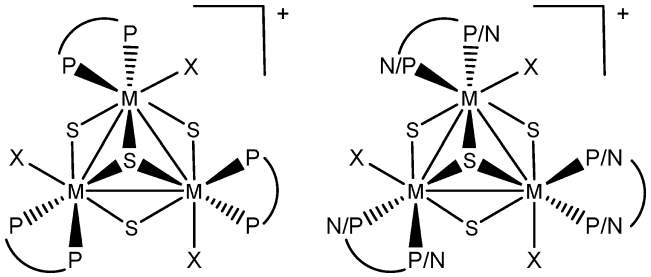

Figure 2. Structures of (left) one of the two enantiomeric forms of $[M_3S_4X_3(diphosphine)_3]^+$ and (right) proposed isomeric structures for $[M_3S_4X_3(aminophosphine)_3]^+$.

isomeric forms are feasible upon the coordination of a bifunctional ligand, such as aminophosphine, to the Mo_3S_4 unit; these assume an analogous coordination to that of the diphosphines, as illustrated in Figure 2.

To promote further development in the field of catalysis, it is essential to understand the substitution reaction mechanisms as well as to gather detailed knowledge of the substrate-binding activation. For example, mechanistic studies on the proton-transfer reaction between trinuclear M_3S_4 (M = Mo, W) diphosphino cluster hydrides and acids support the formation of dihydrogen-bonded adducts, as intermediates or transition states, by the acid attack of the hydrides in the X sites shown in Figure 2.[4,15−17] This finding led us to investigate the catalytic reduction of organic substrates mediated by these trimetallic hydrides. In collaboration with Beller's group, we found that trinuclear Mo_3S_4 hydrides functionalized with outer diphosphane ligands are excellent catalysts for the highly selective reduction of nitroarenes to the corresponding anilines.[9] Tungsten and molybdenum M_3S_4 hydrides bearing diphosphines are also active catalysts in the selective hydrodefluorination of pentafluoropyridine in the *para* position, using silanes as the hydrogen sources.[6] Motivated by the good catalytic performance of the group 8 and group 9 aminophosphino complexes in hydrogenation and transfer-hydrogenation reactions, we decided to design synthesis procedures aimed at functionalizing the highly robust core moiety of the W_3S_4 cluster with aminophosphine ligands.[1,18−26] In particular, we have chosen (2-aminoethyl)-diphenylphosphine (edpp), which bears a NH_2 functional that can serve not only as the coordination group but also as the hydrogen donor or acceptor. This versatility is especially useful in the fields of multifunctional or self-assembled catalysis.

The use of rational synthesis procedures for the preparation of trinuclear metal chalcogenides has contributed enormously to the development of the chemistry of transition-metal clusters. Polymeric one-dimensional ($\{M_3Q_7X_{4/2}X_2\}_n$) phases are the preferred starting material to enter the chemistry of incomplete cubane-type M_3Q_4 clusters containing bidentated phosphines, such as dmpe (1,2-bis(dimethylphosphino)ethane) or dppe (1,2-bis(diphenylphosphino)ethane), as well as optically pure chiral diphosphines, such as Me-BPE (1,2-bis[2,5-(dimethylphospholan-1-yl)] ethane).[5,27,28] In the latter case, the synthesis was revealed to be enantioselective, affording optically pure cluster complexes in almost quantitative yields.

Herein, we present the coordination of edpp to the W_3S_4 cluster unit to afford complexes of $[W_3S_4X_3(edpp)_3]^+$ (X = F, Cl, Br, NCS), which is closely related to $[M_3S_4X_3(diphosphine)_3]^+$ (M = Mo, W) compounds widely investigated in our groups.[5,8,29,30] It is important to note that the kinetics and the mechanism of the substitution reactions in M_3Q_4 clusters have not been studied in detail, except for the case of the aqua clusters that were comprehensively studied by the group of Sykes.[31−35] During the course of the synthesis work with the $[W_3S_4X_3(edpp)_3]^+$ clusters, it was observed that X ligands are easily substituted in acetonitrile solution; this prompted us to carry out a kinetic−mechanistic study of these reactions, combining kinetic experiments and density functional theory (DFT) calculations. The results obtained are reported in this Article and reveal a very rich mechanistic behavior.

EXPERIMENTAL SECTION

General Remarks. Elemental analyses were carried out on a EuroEA3000 Eurovector Analyzer. Electrospray ionization (ESI) mass spectra were recorded with a Quattro LC (quadrupole−hexapole−quadrupole) mass spectrometer with an orthogonal Z-spray electrospray interface (Micromass, Manchester, U.K.). The cone voltage was set at 20 V unless otherwise stated, using CH_3CN as the mobile-phase solvent. Sample solutions were infused at a flow rate of 10 μL/min via a syringe pump that was directly connected to the ESI source, and a capillary voltage of 3.5 kV was used in the positive scan mode. Nitrogen was employed as a drying and nebulizing gas. Experimental isotope patterns were compared with theoretical patterns obtained using MassLynx 4.0 software.[36] $^{19}F\{^1H\}$ and $^{31}P\{^1H\}$ NMR spectra were recorded on Varian Innova 300 and 500 MHz spectrometers, respectively, using CD_3CN as the solvent and referencing to $CFCl_3$ and 85% H_3PO_4, respectively.

Synthesis. All reactions were carried out under a nitrogen atmosphere using standard Schlenck techniques. The solid polymeric phase of $\{W_3S_7Br_4\}_n$ was obtained according to previously published methods.[37] Solvents were dried and degassed by standard methods before use. (2-Aminoethyl)diphenylphosphine (edpp) was obtained from Strem Chemicals and used without further purification.

*$[W_3S_4Br_3(edpp)_3]Br$ (**1**(Br))*. To a suspension of $\{W_3S_7Br_4\}_n$ (0.200 g, 0.183 mmol) in CH_3CN (80 mL) were sequentially added HBr (0.5 M in CH_3CN, 1.3 mL, 0.650 mmol) and edpp (0.275 g, 1.20 mmol) under a nitrogen atmosphere, and the reaction mixture was refluxed for 48 h. The reaction occurred with a color change from brown to blue. After the mixture was cooled to room temperature, the suspension was filtered, the blue solution was concentrated under reduced pressure until one-fourth of its initial volume, and 50 mL of ethanol was added. The desired product was then precipitated with diethyl ether. Finally, the blue solid was separated by filtration and washed with ethanol/diethyl ether (1:10) to yield 0.190 g (62% yield) of an air-stable product characterized as **1**(Br). $^{31}P\{^1H\}$ NMR (CD_3CN, 121 MHz) δ = 15.2 (3P, s, $^1J_{P-W}$ = 93.7 Hz). ESI-MS (CH_3CN, 20 V) m/z: 1607.9 $[M^+]$. Anal. Calcd $W_3Br_4S_4N_3P_3C_{42}H_{48}$: C, 29.9; H, 2.9; N, 2.5. Found: C, 30.2; H, 3.1; N, 2.7.

*$[W_3S_4Cl_3(edpp)_3]Br$ (**2**(Br))*. To a dark-blue solution of **1**(Br) (0.050 g, 0.030 mmol) in CH_3CN (25 mL) was added Pr_4NCl (0.044 g, 0.200 mmol) under a nitrogen atmosphere, and the reaction mixture was stirred for 1 h at room temperature. The reaction occurred with a slight color change from blue to violet. The solution was concentrated under reduced pressure, and the desired product was precipitated by adding diethyl ether. Finally, the blue solid was separated by filtration, washed first with water and then with diethyl ether, and dried under vacuum to yield 0.038 g (82% yield) of an air-stable product characterized as **2**(Br). $^{31}P\{^1H\}$ NMR (CD_3CN, 121 MHz) δ = 18.1 (3P, s, $^1J_{P-W}$ = 92.5 Hz). ESI-MS (CH_3CN, 20 V) m/z: 1474.0 $[M^+]$. Anal. Calcd $W_3Cl_3BrS_4N_3P_3C_{42}H_{48}$: C, 32.5; H, 3.1; N, 2.7. Found: C, 32.8; H, 3.2; N, 3.0.

*$[W_3S_4F_3(edpp)_3]Br$ (**3**(Br))*. This compound was prepared following the general procedure described for **2**(Br), except that Bu_4NF (0.030 g, 0.115 mmol) was reacted with **1**(Br) (0.050 g, 0.030 mmol). The air-stable violet product (0.040 g, 89% yield) was characterized as **3**(Br). $^{31}P\{^1H\}$ NMR (CD_3CN, 121 MHz) δ = 18.3 (3P, d, $^2J_{P-F}$ = 50 Hz). $^{19}F\{^1H\}$ NMR δ = −152.00 (3F, broad signal). ESI-MS (CH_3CN, 20 V) m/z: 1424.1 $[M^+]$. Anal. Calcd $W_3F_3BrS_4N_3P_3C_{42}H_{48}$: C, 33.5; H, 3.2; N, 2.8. Found: C, 33.7; H, 3.5; N, 3.1.

DOI: 10.1021/ic5025313
Inorg. Chem. 2015, 54, 607−618

Table 1. Crystallographic Data for $[1-3](BPh_4)$ and $4_2(PF_6)_2$ Cluster Salts

compound	$1(BPh_4)\cdot(CH_3CN)\cdot(CH_3CH_2OCH_2CH_3)$	$2(BPh_4)\cdot(CH_2Cl_2)$	$3(BPh_4)\cdot(CH_2Cl_2)$	$4_2(PF_6)_2$
empirical formula	$C_{72}H_{71}BBr_3N_4OP_3S_4W_3$	$C_{67}H_{66}BCl_5N_3P_3S_4W_3$	$C_{67}H_{70}BCl_2F_3N_3P_3S_4W_3$	$C_{90}H_{66}F_{12}N_{12}P_8S_{14}W_6$
formula weight	2031.57	1873.99	1828.67	3343.25
crystal system	triclinic	triclinic	triclinic	trigonal
a, Å	14.1815(5)	13.6639(3)	14.2869(3)	16.3126(3)
b, Å	14.9361(5)	15.5155(3)	15.6823(3)	16.3126(3)
c, Å	20.2894(7)	18.3338(3)	17.6782(3)	27.3343(4)
α, deg	101.274(3)	100.7043(14)	75.7547(14)	90.00
β, deg	105.565(3)	100.8016(14)	71.0168(16)	90.00
γ, deg	105.842(3)	108.1880(17)	65.3500(17)	120.00
V, Å^3	3811.6(2)	3500.73(10)	3375.90(10)	6299.22(18)
T, K	199.95(10)	200.00(10)	199.95(10)	293(2)
space group	P-1	P-1	P-1	$P31c$
Z	2	2	2	2
μ(Mo Kα), mm^{-1}	6.304	5.337	5.424	
μ(Cu Kα), mm^{-1}				13.481
reflections collected	40 721	58 146	63 675	36 371
unique reflections/R_{int}	13 412/0.0452	13 744/0.0300	11 862/0.0430	8136/0.0687
goodness of fit (GOF) on F^2	1.073	1.132	1.068	1.134
R_1/wR_2 (all data)[a,b]	0.0417/0.0922	0.0429/0.0840	0.0302/0.0613	0.0485/0.1257
residual ρ/e Å^{-3}	2.73/−0.89	1.77/−1.76	1.62/−0.93	0.92/−0.58

[a] $R_1 = \sum||F_0|-|F_e||/\sum F_0$ [b] $wR_2 = [\sum[w(F_0^2 - F_e^2)^2]/\sum[w(F_0^2)^2]]^{1/2}$

$[W_3S_4(NCS)_3(edpp)_3]Br$ (4(Br)). This compound was prepared following the general procedure described for **2**(Br), except that Bu_4NSCN (0.060 g, 0.200 mmol) was reacted with **1**(Br) (0.050 g, 0.030 mmol). The air-stable blue product (0.041 g, 84% yield) was characterized as **4**(Br). $^{31}P\{^1H\}$ NMR (CD_3CN, 121 MHz) δ = 17.8 (3P, s, $^1J_{P-W}$ = 96.2 Hz). ESI-MS (CH_3CN, 20 V) m/z: 1540.8 [M$^+$]. Anal. Calcd $W_3BrS_7N_6P_3C_{45}H_{48}$: C, 33.3; H, 3.0; N, 5.2. Found: C, 33.7; H, 3.2; N, 5.3.

X-ray Data Collection and Structure Refinement. Suitable crystals for X-ray studies of the tetraphenylborate salts of $\mathbf{1}^+$ were grown by slow vapor diffusion of diethyl ether into a sample solution in CH_3CN. Suitable crystals for X-ray studies of the tetraphenylborate salts of $\mathbf{2}^+$, $\mathbf{3}^+$, and $\mathbf{4}^+$ were grown by slow vapor diffusion of diethyl ether into a sample solution in CH_2Cl_2. Replacement of the Br^- ion was carried out by addition of an excess of $Na(BPh_4)$ to methanol solutions of $[\mathbf{1}-\mathbf{3}](Br)$, resulting in precipitation of the desired tetraphenylborate salts of trinuclear cations $\mathbf{1}^+$ to $\mathbf{3}^+$. Anion exchange, i.e., a Br^- ion for a PF_6^- ion, was carried out by elution with a KPF_6 solution in acetone after absorption of a CH_2Cl_2 solution of **4**(Br) in a silica-gel column.

X-ray diffraction experiments were carried out on an Agilent Supernova diffractometer equipped with an Atlas CCD detector using Mo Kα radiation (λ = 0.71073 Å) for $[\mathbf{1}-\mathbf{3}](BPh_4)$ and Cu Kα radiation (λ = 1.54184 Å) for $\mathbf{4}_2(PF_6)_2$. No instrument or crystal instabilities were observed during data collection. Absorption corrections based on the multiscan method were applied.[38,39] The structures were solved by direct methods in the program SHELXS-97 and refined by the full-matrix method on the basis of F^2 with the program SHELXL-97, using the OLEX software package.[40,41] Details regarding the data collection and the refinement parameters used are listed in Table 1.

The structure of $\mathbf{1}(BPh_4)\cdot CH_3CN\cdot CH_3CH_2OCH_2CH_3$ was refined in triclinic space group P-1. After locating the cluster, eight peaks on general positions remained in the difference Fourier map. These peaks were assigned to carbon, nitrogen, and oxygen atoms from acetonitrile and diethyl ether solvent molecules and refined anisotropically. The structure of $\mathbf{2}(BPh_4)\cdot CH_2Cl_2$ was solved in triclinic space group P-1. Two out of the six carbon atoms of a phenyl substituent from an aminophosphine ligand showed disorder. These were all refined over two positions with a constraint to a total occupancy of one. A disordered CH_2Cl_2 solvent molecule was located in the difference Fourier map where the carbon atom was modeled over two positions with a constraint to a total occupancy of one. The structure of $\mathbf{3}(BPh_4)\cdot CH_2Cl_2$ was refined in triclinic space group P-1. As in the previous structure, the remaining peaks after the location of the cluster and the anion were assigned to carbon and chlorine atoms from a CH_2Cl_2 solvent molecule and refined anisotropically. The structure of $\mathbf{4}_2(PF_6)_2$ was refined in trigonal space group $P31c$ and contains two independent clusters per asymmetric unit with S^c lying on a 3-fold axis. Disorder was observed on two out of the six carbon atoms of a phenyl substituent from an aminophosphine ligand, and these were refined over two positions. Disorder was also observed in one sulfur atom of the thiocyanate ligand, which was also refined over two positions. These were all refined with a constraint to a total occupancy of one. In all cases, anisotropic displacement parameters were refined for all non-H atoms except for the disordered carbon atoms. The hydrogen atoms bonded to carbon were included at their idealized positions and refined as riders with isotropic displacement parameters assigned as 1.2 times the U_{eq} value of the corresponding bonding partner. The structural figures were drawn using Diamond (a visual crystal-structure-information software system).[42]

Kinetic Experiments. The kinetic experiments were carried out with an Applied Photophysics SX-17MV stopped-flow spectrometer provided with a PDA1 photodiode array (PDA) detector. All experiments were carried out at 25.0 °C. The reactions of $[W_3S_4X_3(edpp)_3]Br$ (X = Br^- ($\mathbf{1}^+$),Cl^- ($\mathbf{2}^+$), F^- ($\mathbf{3}^+$), or NCS^- ($\mathbf{4}^+$)) clusters (~2×10^{-4} M) with different entering ligands (Cl^-, Br^-, F^-, NCS^-) were studied using acetonitrile as the solvent. We used a range of concentrations between 8.3×10^{-3} and 0.05 M. Measurements were carried out under the condition of ionic strength = 0.05 M. In each case, a salt of the halide (X^- of the complex) was used. We found that the results were similar with or without the added salt, but the quality of the fits was better if salt was not present. In all cases, the spectral changes were measured over a wide wavelength range and analyzed with SPECFIT/32 software,[43] using the kinetic models indicated in the corresponding section.

DFT Calculations. DFT calculations were conducted with the Becke hybrid density functional (B3LYP)[44] method, as implemented in the Gaussian 09 program suite.[45] The double-ξ pseudo-orbital basis set LanL2DZ, in which W, H, C, N, P, S, F, Cl, and Br are represented as the relativistic core LanL2 potential of Los Alamos, was used. B3LYP/LanL2DZ has been proven a reliable tool for describing geometric and electronic structures as well as the energy profiles of M_3S_4 (M = Mo,W) clusters.[16,46,47] The three potential energy surfaces (PESs) were obtained for the substitution of one of the bromides of $\mathbf{1}^+$ by the entering ligands in each case by constructing a grid with varying W−Br and W−X distances and optimizing fully the remaining geometric

DOI: 10.1021/ic5025313
Inorg. Chem. 2015, 54, 607−618

parameters. In three cases, the W−Br distance was varied from the bonding distance (2.72 Å) to 4.72 Å in 0.2 Å steps. The W−X distances were increased by 2 Å in 0.2 Å steps, starting from the corresponding bonding distances (2.02 Å for W−F, 2.55 Å for W−Cl, and 2.04 Å for W−NCS). Therefore, a total of 11 × 11 points, i.e., 121 points, have been calculated to construct each potential energy surface. The geometry optimizations were first carried out in gas phase without any symmetry constraint, followed by analytical frequency calculations to confirm that a minimum or a transition state had been reached. The nature of the species connected by a given transition-state structure was checked by calculating the intrinsic reaction coordinate (IRC) pathway;[48] this ensures that the transition structure (TS) connects to the reactant and product complexes following the transition vector downhill from the corresponding TS. Taking the calculated gas-phase structures as starting points, we also conducted geometry optimizations without any constraints, using the polarizable continuum model (PCM) approach[49,50] to include the acetonitrile solvent effect in the geometries and energies. We considered electronic energies and Gibbs free energies for discussion. The latter have been obtained by means of frequency calculations of the stationary points found at room temperature.

RESULTS AND DISCUSSION

Synthesis, Molecular Structure, and Reactivity. The excision reaction of $\{W_3S_7Br_4\}_n$ polymeric phases with an excess of edpp ($PPh_2(CH_2)_2NH_2$) in acetonitrile in the presence of HBr (eq 1) affords only one of all of the possible isomers of formula $[W_3S_4Br_3(edpp)_3]^+$ ($\mathbf{1}^+$) in a single synthesis step and good yields (ca. 60%).

$$\{W_3S_7Br_4\}_n + 6PPh_2(CH_2)_2NH_2(edpp) \xrightarrow{HBr} [W_3S_4Br_3(edpp)_3]Br + 3SPPh_2(CH_2)_2NH_2 \quad (1)$$

The substitutional reactivity of the W−Br bond in $[W_3S_4Br_3(edpp)_3]^+$ toward halide and pseudohalide salts (eq 2) also allowed us to prepare and fully characterize the fluoride, chloride, and thiocyanate tungsten derivatives of $[W_3S_4X_3(edpp)_3]^+$ (X = F, Cl, NCS) in high yields.

$$[W_3S_4Br_3(edpp)_3]Br + 3X^- \rightarrow [W_3S_4X_3(edpp)_3]Br + 3Br^- \quad (2)$$

The structures of cations $[W_3S_4Br_3(edpp)_3]^+$ ($\mathbf{1}^+$), $[W_3S_4Cl_3(edpp)_3]^+$ ($\mathbf{2}^+$), $W_3S_4F_3(edpp)_3]^+$ ($\mathbf{3}^+$), and $[W_3S_4(NCS)_3(edpp)_3]^+$ ($\mathbf{4}^+$) have been determined by the single-crystal X-ray diffraction of their tetraphenylborate or hexafluorophosphate salts, and they share structural features. The four cations contain the incomplete-cuboidal cluster W_3S_4, which results from the reduction of the disulfide bridges (present in the starting polymeric bromide material) to sulfides. In this unit, the tungsten and sulfur atoms occupy adjacent vertices in a cube with a metal position missing, which results in an incomplete cubane-type structure. Figure 3 shows two ORTEP views of cation $\mathbf{1}^+$. In $\mathbf{4}^+$, the three outer thiocyanate ligands occupy the halide positions in $\mathbf{1}^+$ to $\mathbf{3}^+$, and these coordinate the metal through the nitrogen atom. The packing of $\mathbf{4}(PF_6)$ occurs with two crystallographycally independent trimetallic cluster units and short NCS···HN contacts (2.420 Å) between the sulfur atom of a thiocyanate ligand on one cluster and the hydrogen atom of the amino group of the adjacent cluster. Table 2 contains a list of the most important averaged bond lengths for cations $\mathbf{1}^+$ to $\mathbf{4}^+$ as well as those reported for $[W_3S_4Br_3(dmpe)_3]^+$ for comparative purposes.[51] The three metal atoms define an approximately equilateral triangle with W−W bond distances of 2.7520[3] Å for $\mathbf{1}^+$, 2.7495[3] Å for $\mathbf{2}^+$, 2.7357[3] Å for $\mathbf{3}^+$ 2.7507[11] Å for $\mathbf{4}^+$, which is in agreement with the presence of a single metal−metal bond. The nature of $W(\mu_3\text{-}S)(\mu_3\text{-}S)_3$ is such

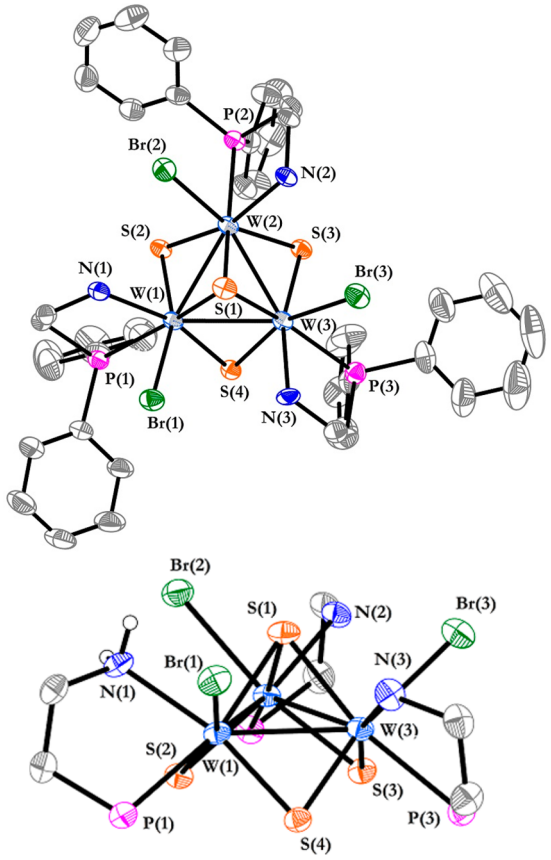

Figure 3. ORTEP representations of two different views of cation $\mathbf{1}^+$ (ellipsoids = 50% probability). (top) Hydrogen atoms have been omitted for clarity. (bottom) Phenyl rings and hydrogen atoms, except those directly bonded to N(1), have been also omitted to emphasize the halogen and H_2−N orientations.

that S^b and S^c occupy a set of facial positions around the pseudo-octahedrally coordinated metal atoms, leaving the three outer facial sites available for the phosphorus and nitrogen atoms of the aminophosphine and a site occupied by the halide ligand. Remarkably, as previously mentioned, only one isomer is formed, wherein all three nitrogen atoms of the amino groups are located trans to S^b and the three phosphorus atoms are located trans to S^c. A similar situation is found in $M_3Cl_4(H_2O)_2(PPh_3)_3$ complexes that result from the substitution of water molecules by PPh_3 in acidic HCl solutions of $[M_3S_4(H_2O)_9]^{4+}$ aquo ions.[52] Kinetic studies by Sykes and co-workers give different labilities for the three outer metal positions present in $[M_3S_4(H_2O)_9]^{4+}$ aquo ions, with the two positions trans to S^b being 10^5 times more labile than those trans to S^c.[34] In the M_3S_4 system, the ligand's harder atoms have a tendency to occupy the more labile positions so that the nitrogen atom of the aminophosphine is located trans to S^b. Therefore, the nitrogen and halogen atoms coordinated to the same metal center are found on the same side of the trimetallic plane, as shown in the bottom of Figure 3, with X···N distances of 3.021, 3.015, 2.723, and 2.728 Å for $\mathbf{1}^+$, $\mathbf{2}^+$, $\mathbf{3}^+$, and $\mathbf{4}^+$, respectively. However, the shorter X···H(−N) distances in $\mathbf{1}^+$ and $\mathbf{2}^+$ correspond to X···H interactions between the halogen atoms and amino groups on adjacent metals, with values ranging from 2.745 to 2.859 Å for $\mathbf{1}^+$ and from 2.529 to 3.048 Å for $\mathbf{2}^+$. In the case of fluorocomplex $\mathbf{3}^+$, the above X···H(−N) distances (2.469 to 2.829 Å) are comparable to the X···H(−N) interactions between the halogen atoms and amino groups on the

DOI: 10.1021/ic5025313
Inorg. Chem. 2015, 54, 607−618

Table 2. Selected Averaged Bond Distances (Å) for [1−3](BPh$_4$), 4(PF$_6$), and [W$_3$S$_4$Br$_3$(dmpe)$_3$](PF$_6$)

length (Å)[a]	[W$_3$S$_4$Br$_3$(dmpe)$_3$](PF$_6$)[51]	**1**(BPh$_4$)	**2**(BPh$_4$)	**3**(BPh$_4$)	**4**(PF$_6$)
W−W	2.759(2)	2.7520[3]	2.7495[3]	2.7357[3]	2.7507[11]
W−μ_3-S(1)	2.37(1)	2.3450[16]	2.3715[15]	2.3769[13]	2.371[3]
W−μ-S(2)[b]	2.30(1)	2.3117[15]	2.3104[15]	2.3140[13]	2.315[3]
W−μ-S(2)[c]	2.33(1)	2.3091[15]	2.3040[15]	2.3066[13]	2.298[3]
W−P(1)[d]	2.51(1)	2.5306[16]	2.5408[17]	2.5264[14]	2.542[4]
W−N		2.286[5]	2.268[5]	2.267[4]	2.276[11]
W−X (X = F, Cl, Br, NCS)	2.641(4)	2.6401[7]	2.4947[16]	2.043[4]	2.114[10]

[a]Standard deviations for averaged values are given in square brackets. [b]W−μ-S distance trans to W−X bond. [c]W−μ-S distance trans to W−P ([W$_3$S$_4$Br$_3$(dmpe)$_3$]$^+$) or W−N ([**1**−**3**](BPh$_4$)) bond. [d]W−μ-S distance trans to the W−(μ_3-S) bond.

same metal center, with values ranging from 2.464 to 2.673 Å. For **4**$^+$, the shorter X···H(−N) distances correspond to interactions between nitrogen atoms, i.e., between the NCS$^-$ ligand and amino groups on the same metal center, with values ranging from 2.661 to 2.665 Å.

The solid-state structure of complexes **1**$^+$−**4**$^+$ is preserved in solution, as evidenced by their ^{31}P{^{1}H} NMR spectra registered in CD$_3$CN that show a single signal at 15.2 ppm for **1**$^+$, 18.1 ppm for **2**$^+$, and 17.8 ppm for **4**$^+$; this is in agreement with the presence of three equivalent phosphorus nuclei. The phosphorus signal for **3**$^+$ appears as a doublet that is centered at 18.3 ($^2J_{P-F}$ = 50 Hz) ppm, a result of the coupling between the phosphorus and fluorine nuclei. The ESI mass spectra of the halide amoniphosphine complexes show one peak centered at 1607.9, 1474.0, 1424.1, and 1540.8 m/z for **1**$^+$, **2**$^+$, **3**$^+$, and **4**$^+$, respectively, each of which is attributed to the respective pseudomolecular cation on the basis of the m/z value and the cation's characteristic isotopic pattern. As for the family of [M$_3$Q$_4$X$_3$(diphosphine)$_3$]$^+$ (M = Mo, W; Q = S, Se, and X = F, Cl, Br, and H) complexes, this spectrometric technique has been very useful for the characterization of the new aminophosphine cluster complexes.

Reactivity studies show that the substitution of the bromides in **1**$^+$ by Cl$^-$ or NCS$^-$ easily occurs at room temperature, which contrasts with earlier observations in the diphosphino W$_3$S$_4$ system where no reaction is observed.[53] Only the substitution of bromide by fluoride occurs for both the diphosphino and the aminophosphino (L) trimetallic [W$_3$S$_4$Y$_3$L$_3$]$^+$ clusters.

The reaction of **1**$^+$ with halide or pseudohalide salts was monitored by ESI mass spectrometry and ^{31}P{^{1}H} NMR, and the sequential substitution of bromide by chloride, fluoride, or thiocyanate ligands was observed. Thus, in the case of the reaction between **1**$^+$ and Cl$^-$, the sequential substitution of the terminal ligands is demonstrated by the appearance of peaks at m/z = 1563.7, 1517.8, and 1474.0 in the ESI-MS monitoring of [W$_3$S$_4$Br$_2$Cl(edpp)$_3$]$^+$, [W$_3$S$_4$BrCl$_2$(edpp)$_3$]$^+$, and [W$_3$S$_4$Cl$_3$(edpp)$_3$]$^+$, respectively (Figure 4). Similar data are obtained by monitoring the reaction with phosphorus NMR. These results are summarized in Figure 5, and they show that the conversion of **1**$^+$ to **2**$^+$ occurs via the formation of two reaction intermediates. Although the spectra of the starting complex and the reaction product each consist of a single signal (A and D, respectively, in Figure 5), the spectra of the intermediates contain three signals, labeled B for the first intermediate and C for the second, indicating that the three edpp ligands are no longer equivalent in the intermediates [W$_3$S$_4$Br$_2$Cl(edpp)$_3$]$^+$ and [W$_3$S$_4$BrCl$_2$(edpp)$_3$]$^+$. The facile substitution at room temperature of the bromide ligand in **1**$^+$ by other halides or pseudohalides is a distinctive feature of the W$_3$S$_4$ amino-

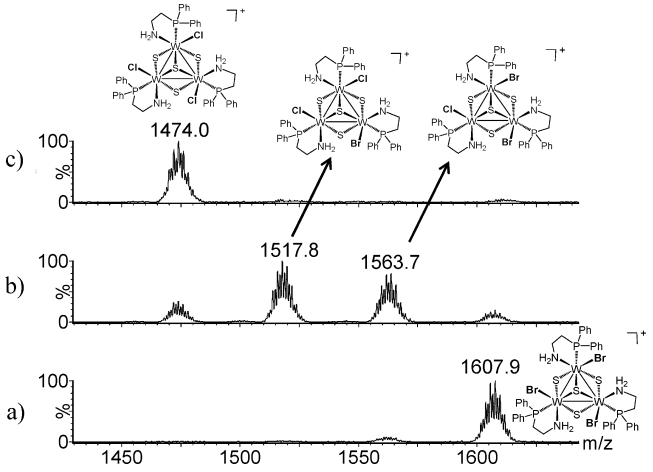

Figure 4. ESI-MS monitoring of the reaction between **1**$^+$ and Pr$_4$NCl. (a) Initial time, (b) after 3 min, and (c) after 1 h.

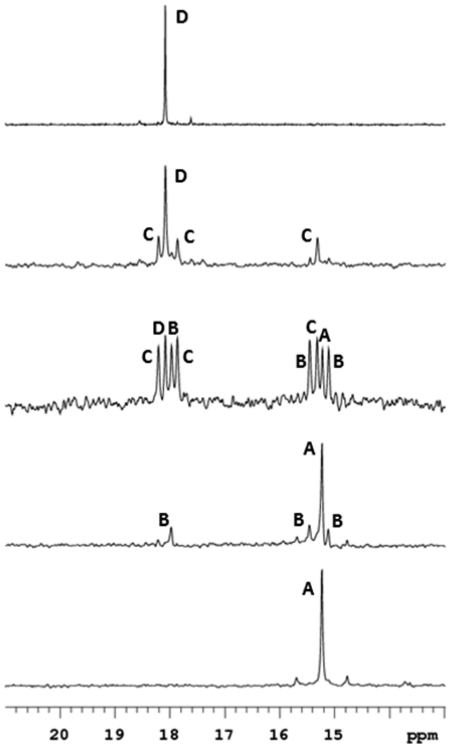

Figure 5. ^{31}P {^{1}H} NMR spectra of (A) **1**$^+$, (B) first intermediate, (C) second intermediate, and (D) **2**$^+$ in the sequential reaction of **1**$^+$ with Pr$_4$NCl in acetonitrile-d_3, obtained through the addition of successive aliquots of a solution of the chloride salt (bottom to top).

DOI: 10.1021/ic5025313
Inorg. Chem. 2015, 54, 607−618

phosphino complex when compared with its diphosphino analogues.

Quite similar results are also observed during the reaction of $\mathbf{1}^+$ with F^- and NCS^-; the positions of the NMR signals are shown in Table 3. For the reaction with fluoride, the phosphorus spectra

Table 3. Chemical Shifts of the $^{31}P\{^1H\}$ Signals (ppm) in CD_3CN at 25.0° C for the Species Formed in the Reaction of $\mathbf{1}^+$ with Different Incoming Ligands

X	W_3Br_3	W_3Br_2X	W_3BrX_2	W_3X_3
Cl^-	15.2	15.1, 15.4, 18.0	15.3, 17.9, 18.2	18.1
NCS^-		(15.2, 15.4), 18.0[a]	(15.4), 17.6, 18.1[a]	17.8
F^-		*b*	*b*	18.3 ($^2J_{F,P}$ = 50 Hz)

[a]Signals in parentheses overlapped with those of the starting material and the other intermediate. [b]It has not been possible to assign the signals corresponding to the reaction intermediates because broad unresolved signals are observed.

are complicated by the existence of coupling with the coordinated fluorides, which leads to the splitting of the signals and thus hinders a detailed assignment of the signals for the different intermediates. In any case, a doublet with a P−F coupling constant of 50 Hz was observed for the trisubstituted species. Interestingly, the $^{19}F\{^1H\}$ spectrum shows a broad signal centered at −152 ppm, and the coupling with the phosphorus nuclei could not be resolved even at a low temperature. Broadening of the $^{19}F\{^1H\}$ NMR signal in fluorido complexes containing nitrogen donor ligands is not unprecedented;[54] in the present case, it could be associated with some interaction of coordinated fluoride with the neighboring amino groups. In addition to the signals in Table 3, the NMR spectra recorded at long reaction times usually reveal the appearance of a series of less-intense signals at 30−40 ppm, which probably correspond to some secondary or decomposition product.

Table 3 lists the $^{31}P\{^1H\}$ chemical shifts for the species formed in the reaction of $\mathbf{1}^+$ with different incoming ligands and supports the formation of two intermediates between $\mathbf{1}^+$, with three W−Br bonds, and the reaction product, with three W−X bonds. For a given intermediate, the number of signals with chemical shifts close to that observed for $\mathbf{1}^+$ (15.2 ppm) coincides with the number of Br ligands in the intermediate, i.e., two for the first intermediate and one for the second, which suggests that those signals correspond to the edpp ligands coordinated to the metal centers with unreacted W−Br bonds. Furthermore, the remaining signals of the intermediates correspond to edpp ligands coordinated to metal centers via W−X bonds, and they appear at chemical shifts closer to that observed for the trisubstituted W−X reaction product. It is also interesting that the symmetry is recovered and that the three edpp ligands become equivalent once the reaction is completed by the substitution at the third metal center, indicating that all the edpp ligands retain their original disposition, i.e., that of the three P donors at the same site of the plane defined by the three metal centers. From the mechanistic point of view, this indicates that the entering ligand approaches the metal center at the proximities of the W−Br bond, with the entering ligand finally occupying the coordination site initially occupied by the leaving bromide.

Experiments similar to those described above were carried out with other starting complexes. These experiments showed that fluorocomplex $\mathbf{3}^+$ does not react with an excess of any of the other three entering ligands (Cl^-, Br^- or NCS^-); this suggests that it is the most thermodynamically stable. In agreement with this conclusion, both $\mathbf{2}^+$ and $\mathbf{4}^+$ were found to react with an excess of fluoride. More details about the kinetic results are given below.

Kinetics of Substitution Reactions. The kinetics of the reactions of $[W_3S_4X_3(edpp)_3]Br$ (X = Br^-, Cl^-, F^-, NCS^-) clusters with an excess of the different entering ligands (Cl^-, Br^-, F^-, or NCS^-) was studied in acetonitrile. In general, the spectral changes observed under pseudo-first-order conditions for the reactions in eq 3 show that the conversion of the starting complex to the trisubstituted compound occurs within the time scale of the stopped-flow technique, although in most cases there are additional slower changes that surely correspond to the secondary or decomposition process also detected in the ESI-MS and NMR studies. In agreement with the NMR observations mentioned above, trifluoro cluster $\mathbf{3}^+$ did not show any substitution reactions with any of the other ligands because of its higher stability. The kinetics of interconversion between the tribromo and trichloro complexes ($\mathbf{1}^+$ and $\mathbf{2}^+$) could not be studied because the spectral changes are very small and overlap with those for secondary processes so that all attempts to analyze the kinetic data led to unreproducible results.

$$[W_3S_4X_3(edpp)_3]Br + 3Y^- \rightarrow [W_3S_4X_3(edpp)_3]Br + 3X^- \quad (3)$$

As an example of the reactions studied, the spectral changes observed for the reaction of $\mathbf{1}^+$ with F^- are illustrated in Figure 6,

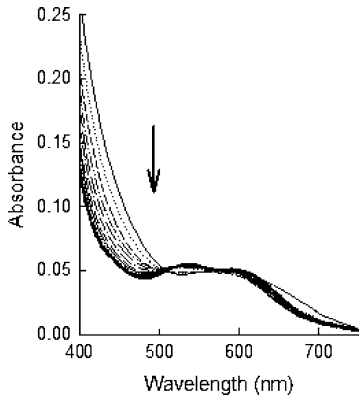

Figure 6. Typical spectral changes for the reaction of $\mathbf{1}^+$ with Bu_4NF, yielding $\mathbf{3}^+$ in acetonitrile at 25.0 °C (cluster concentration = 5×10^{-5} M, $[Bu_4NF]$ = 0.025 M, experiment time = 0.4 s).

and the other cases are included in the Supporting Information. In general, the changes can be satisfactorily fitted to a kinetic model with a single exponential (A → B); the fit leading to the calculated spectra of A and B agrees well with those recorded for the solutions of clusters $\mathbf{1}^+$ to $\mathbf{4}^+$. The observation of a single kinetic step for the overall process of sequential reaction at the three metal centers is quite common in the kinetic studies of these kinds of compounds, and it can be rationalized by considering that the process occurs with statistically controlled kinetics.[4,16,33,35] Thus, if the three metal centers behave independently of each other, then it must be expected that the rates of substitution of the three X monodentate ligands in Figure 2 will be controlled by the statistics and the three consecutive kinetic steps will show rate constants in a ratio of 3:2:1. However, if the three metal centers also behave as independent chromophores the rate law is simplified and the kinetic traces only show a single resolvable step. The requirements for this

DOI: 10.1021/ic5025313
Inorg. Chem. 2015, 54, 607−618

simplification of the kinetics as well as the reasons leading to possible deviations from the statistical behavior have been recently discussed.[55]

The dependence of the values of the observed rate constant (k_{obs}) on the concentration of the entering ligand is illustrated for the reaction of $\mathbf{1}^+$ with F^- and NCS^- in Figures 7 and 8. Although

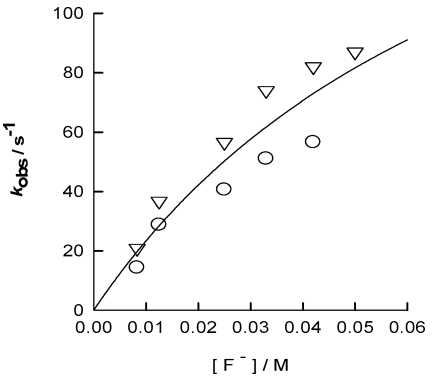

Figure 7. Plot showing $[F^-]$ dependence of the observed rate constant for the reaction of $\mathbf{1}^+$ with F^- to form $\mathbf{3}^+$: (▽) reaction with added Br^- and (○) reaction with no added Br^-. In experiments with added Br^-, the sum of the concentrations of both anions is 0.05 M. The solid line corresponds to the fit of all the data using eq 5.

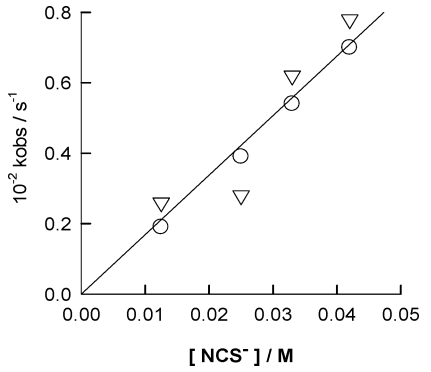

Figure 8. Plot showing the $[NCS^-]$ dependence of the observed rate constant for the reaction of $\mathbf{1}^+$ with NCS^- to form $\mathbf{4}^+$: (▽) reaction with added Br^- and (○) reaction with no added Br^-. In experiments with added Br^-, the sum of the concentrations of both anions is 0.05 M. The solid line corresponds to the fit of data using eq 4.

the data for the thiocyanate reaction can be satisfactorily fitted to a straight line (eq 4, with $a = 0.16 \pm 0.01\ M^{-1}\ s^{-1}$), the reaction with fluoride shows saturation kinetics (eq 5, with $a = (2.6 \pm 0.6) \times 10^3\ M^{-1}\ s^{-1}$ and $b = 12 \pm 9\ M^{-1}$). However, eq 4 can be considered to be a simplification of eq 5. The effect of the leaving ligand on the kinetics of reaction was checked by studying the reaction of $\mathbf{1}^+$ with fluoride or thiocyanate in the presence of bromide. As shown in Figures 7 and 8, in no case is there the deceleration expected for a dissociative mechanism. In both cases, the results are quite close to those obtained in the absence of bromide, and the values of a and b above have actually been obtained by fitting together the data in the absence and presence of the leaving ligand. With fluoride, the reaction is somewhat faster in the presence of added bromide. Although these differences could be associated with competition between the anions to form the different productive and unproductive outer-sphere complexes mentioned below, the kinetic differences are not large, which hinders a detailed analysis. In any case, these results clearly rule out a dissociative mechanism in which the leaving ligand dissociates before the entering ligand approaches the metal center.

$$k_{obs} = a[NCS^-] \tag{4}$$

$$k_{obs} = \frac{a[F^-]}{1 + b[F^-]} \tag{5}$$

The kinetic data for the substitution of coordinated bromide reveal that changing the nature of the entering ligand leads to a variety of rate laws and to changes in the numerical values of the rate constants by several orders of magnitude. These findings can be explained by the mechanism depicted in eqs 6−8, in which there is a rapid preequilibrium that leads to the formation of an outer-sphere complex between the cluster and the entering ligand that is followed by a rate-determining ligand exchange.

$$\mathbf{Br{-}M^+} + Y^- \rightleftarrows (Br{-}M^+\cdots Y^-); \qquad K_{os} \tag{6}$$

$$(\mathbf{Br{-}M^+}\cdots Y^-) \rightarrow (\mathbf{Y{-}M^+}\cdots Br^-); \qquad k_2 \tag{7}$$

$$(\mathbf{Y{-}M^+}\cdots Br^-) \rightarrow \mathbf{Y{-}M^+} + Br^- \qquad ; \text{fast} \tag{8}$$

The rate law for this mechanism is given by eq 9, which has the same form as eq 5 with the equivalencies $a = k_2K_{os}$ and $b = K_{os}$. Depending on the value of the product $K_{os}[Y^-]$, the rate law can be simplified to single first-order dependence with respect to Y. From the experimental values of a and b, it can be concluded that the kinetic differences observed for these substitutions can be associated with changes in any of the k_2 or K_{os} terms.

$$k_{obs} = \frac{k_2K_{os}[Y^-]}{1 + K_{os}[Y^-]} \tag{9}$$

The reaction of clusters $\mathbf{2}^+$ and $\mathbf{4}^+$ with F^- showed results quite close to those observed for the analogous reaction of $\mathbf{1}^+$, with $a = (2.0 \pm 0.3) \times 10^3\ M^{-1}\ s^{-1}$ and $b = 33 \pm 8\ M^{-1}$ for the substitution of Cl^- and $a = (2.1 \pm 0.2) \times 10^4\ M^{-1}\ s^{-1}$ and $b = 180 \pm 12\ M^{-1}$ for the substitution of NCS^-. The reaction of $\mathbf{2}^+$ with NCS^- showed very small spectral changes (Supporting Information); the magnitude of these increased slightly when the concentration of NCS^- increased. As a consequence of these small changes, the dependence of the observed rate constants on the concentration of thiocyanate is not clear, although it can be considered to be independent of the concentration of NCS^- with a value of $k_{obs} = 0.040 \pm 0.007\ s^{-1}$. These results suggest that the reaction occurs under conditions of reversibility, which is further supported by experiments with added Cl^-, indicating that the presence of the leaving ligand inhibits the reaction. In that case, the values of k_{obs} would include contributions of the rates on both directions and the dependence on the concentration of leaving and entering ligands would not be well defined because of the small changes. Quite similar conclusions were reached when studying the kinetics of the reaction in the reverse direction, i.e., the substitution of thiocyanate by chloride. In that case, there is no reaction upon addition of the leaving ligand (NCS^-), but a reaction is observed when Cl^- is the only anion added to the reaction medium. Nevertheless, the small amplitude of the absorbance changes again hinders a satisfactory kinetic analysis. When taken together with the rest of the observations in the present Article, it can be concluded that the stability of the complexes follows the order $\mathbf{1}^+ < \mathbf{2}^+ \approx \mathbf{4}^+ < \mathbf{3}^+$, i.e., the maximum stability is achieved with the F^- ligand (not substituted by an excess of any of the other ligands) and the least stable is the Br^-

DOI: 10.1021/ic5025313
Inorg. Chem. 2015, 54, 607−618

complex (easily substituted by all the other anions). The chloride and NCS^- complexes are ranked between the other two halides, and their stabilities are close to each other.

From the kinetic point of view, the two most striking observations are the rapidity of the reaction and the wide range of values observed for the rate constants, which spans several orders of magnitude. The dependence of the rate on the concentration of the entering ligand and the lack of dependence on the concentration of the leaving ligand can best interpreted by considering that substitutions have an associative character. We have recently found that ligand substitutions in this kind of cluster can also go through a particular associative mechanism in which the excess of electron density caused by the attack by the entering ligand is compensated for by the reorganization of the cluster core without the dissociation of the leaving ligand (Figure 9).[4,17] The entering ligand (Y) coordinates to the metal center

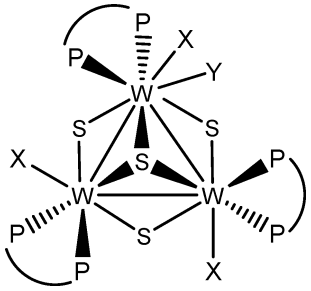

Figure 9. Proposed structure for the intermediate formed in associative substitution of X by Y in M_3S_4 clusters.

without the dissociation of the leaving ligand (X), and the process is accompanied by structural changes in the cluster core.

DFT Calculations. To gain insight into the intimate mechanism of these substitution reactions, DFT calculations were carried out using cluster $\mathbf{1}^+$ as a starting model. The geometry of the cluster optimized at the B3LYP/LanL2DZ level (Supporting Information) compares well with that resolved by X-ray diffraction; the differences generally range from 1.2 to 5%. The study of the substitution processes has been carried out at a single metal center, an approach that has been successfully employed in other theoretical studies.[6,16,17] We use the prime symbol to designate the compounds resulting from this single-center substitution. For instance, $\mathbf{2}^{+\prime}$ refers to the cluster resulting from the substitution of one of the bromide ligands of $\mathbf{1}^+$ by a chloride ligand, i.e., $[W_3S_4Br_2Cl(edpp)_3]^+$.

The energy values calculated in acetonitrile solution for the different substitutions starting from cluster $\mathbf{1}^+$ are included in Table 4, and they compare very well with the experimental results: The most stable compound is the fluoride complex, whereas the least stable is the bromide adduct. The clusters containing Cl^- and NCS^- are close in energy to one another.

The next step was to construct PESs for the substitution of one of the bromides by the different Y^- entering ligands: Cl^-, F^-, and

Table 4. Summary of the Energies (ΔE) and Gibbs Free Energies (ΔG) Calculated in Acetonitrile Solution for the Different Substitution Reactions in Cluster $\mathbf{1}^+$

reaction	ΔE (kcal/mol)	ΔG (kcal/mol)
$\mathbf{1}^+ + Cl^- \rightleftharpoons \mathbf{2}^{+\prime} + Br^-$	−11.2	−9.3
$\mathbf{1}^+ + F^- \rightleftharpoons \mathbf{3}^{+\prime} + Br^-$	−48.1	−45.5
$\mathbf{1}^+ + NCS^- \rightleftharpoons \mathbf{4}^{+\prime} + Br^-$	−15.2	−9.8

NCS^-. Because the kinetic data rules out a limiting dissociative mechanism in which Br^- leaves the coordination site before the approach of the entering ligand, ($\mathbf{1}^+$, Y^-) adducts with Y^- approaching one of the W centers at the proximities of the W−Br bond were used as the starting point for modeling the PES corresponding to the substitution process. This approach is also based on the NMR observations indicating that the entering ligand approaches the metal center in the same direction as the leaving ligand. The final point in those calculations was the adduct that results from the release of Br^- from $\mathbf{1}^+$ to afford $\mathbf{2}^{+\prime}$, $\mathbf{3}^{+\prime}$, or $\mathbf{4}^{+\prime}$. The calculated surfaces are shown in Figure 10 and indicate a rich mechanistic chemistry for these substitutions.

In the case of fluoride as the entering ligand (Figure 10a), an associative interchange of the ligands is predicted for the bromide substitution: the minimum energy path (MEP) from the left (reactants) to the right (products) corners of the PES begins with a shortening of the W−F distance without a concomitant lengthening of the W−Br distance. The point of maximum energy of the MEP shows W−F and W−Br distances of 2.82 and 2.92 Å, respectively, and it was used as the starting point for calculating the corresponding transition state (TS), whose geometry is depicted in Figure 11a. The W−F distance is now 2.92 Å, which is slightly longer than the one predicted from the PES, and the W−Br distance is only 2.77 Å at the TS, which is essentially the same as the W−Br distances in the other two metallic centers (2.75 and 2.77 Å). Hence, the associative character of the ligand exchange is confirmed, even strengthened, when the true TS is found. The geometry of the TS shows that the bond distances between W and S^c and between W and the S^b trans to the NH_2 group essentially remain unchanged upon addition of the fluoride, whereas the W−(μ-S) distance trans to the leaving Br increases from 2.36 Å to 2.38−2.48 Å. Thus, it appears that the excess electron density introduced by the entering ligand is accommodated by the weakening of the trans W−S bond. Intrinsic reaction coordinate (IRC) calculations from the TS led to adducts whose optimized structures are shown in Figure 12. These structures indicate that outer-sphere complexes form between the cluster and the anion, which is in agreement with previous reports on related systems.[56] The stability of the different outer-sphere complexes can be estimated from the relative energy values, listed in Table 5, with regard to those of the separated ions. In general, the free energies are close to zero, except for that of the ($\mathbf{1}^+$, F^-) adduct (Figure 12), which is significantly more stable than the other outer-sphere complexes. A detailed inspection of the geometry reveals that F^- approaches the cluster at the proximities of the amino group of the edpp ligand coordinated to the adjacent W in such a way that there is a such strong interaction with one of the H atoms (H···F distance = 1.02 Å) that it is almost extracted from the edpp ligand. In the other outer-sphere complex, ($\mathbf{3}^+$, Br^-), the anion also interacts with one hydrogen of an amino group, but the interaction is much weaker (H···Br distance of ca. 2 Å). The importance of the H···F interaction is also evident in the corresponding transition state (Figure 11a), which shows an H···F distance of 1.37 Å, clearly suggesting that the entering of fluoride is assisted by the hydrogen atom of the amino moiety of the vicinal edpp.

The energies in Table 5 anticipate that in solution the equilibrium between the free cluster and the outer-sphere complex would be displaced toward the latter species when the entering ligand is F^- but to the free cluster for other ligands. Although the outer-sphere complexes mentioned above correspond to Y^- approaching the W center in a particular

DOI: 10.1021/ic5025313
Inorg. Chem. 2015, 54, 607−618

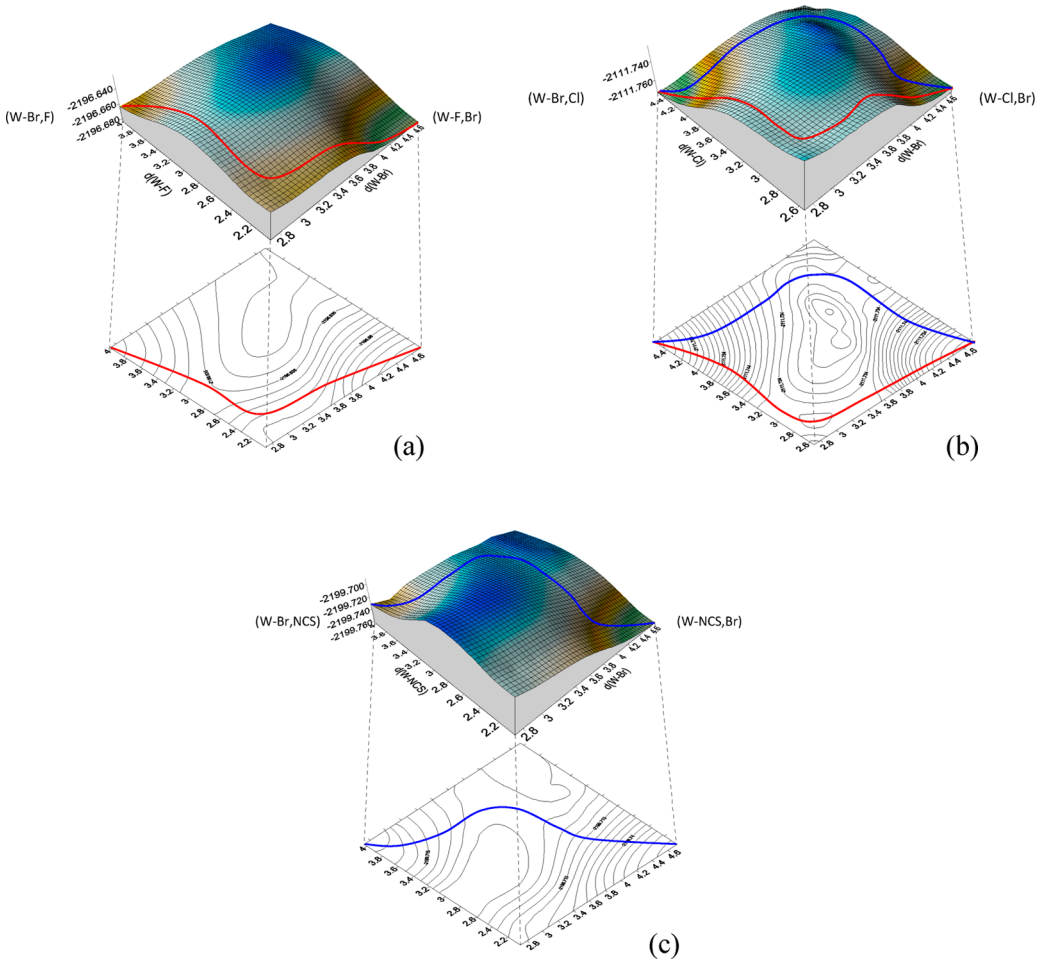

Figure 10. Potential energy surfaces for the substitution of one of the Br^- of $\mathbf{1}^+$ by different entering ligands (Y^-). The absolute energy (hartrees per particle) is depicted as a function of the W−Br and W−Y distances (angstroms), and Y^- = (a) F^-, (b) Cl^-, or (c) NCS^-. The surfaces have been depicted in such a way that $\mathbf{1}^+ + Y^-$ is always located on the left corner, whereas $\mathbf{3}^{+\prime}$, $\mathbf{2}^{+\prime}$, or $\mathbf{4}^{+\prime}$ (a, b, and c, respectively) + Br^- are always located on the right corners as indicated. The minimum energy paths have been sketched (red lines, associative pathways; blue lines, dissociative pathways).

orientation that favors the substitution process, other orientations are also possible for the entering anions, as found experimentally for related systems.[56] Because the outer-sphere complexes with these alternative structures are usually unable to evolve into the substitution product, they would represent dead-end species that would simply compete with the productive outer-sphere complexes and thus slow down the reaction. Although the formation of these alternative outer-sphere complexes has not been explored in detail, several possibilities have been analyzed as shown in Figure 12. Structures $(\mathbf{1}^+, F^-)_B$ and $(\mathbf{3}^{+\prime}, Br^-)_B$ were obtained by approaching the uncoordinated anion to the cluster at the proximities of the three NH_2 groups. Again, the strong interaction of fluoride with one of the H atoms is revealed in the case of $(\mathbf{1}^+, F^-)_B$. Structures $(\mathbf{1}^+, F^-)_C$ and $(\mathbf{3}^{+\prime}, Br^-)_C$ were obtained by approaching the anion at the proximities of the three bridging sulfurs, with the outer-sphere complex being less stable in this case. In most cases, the energy values (Table 5) for various productive and unproductive outer-sphere complexes are similar.

Table 5 also includes the values of $\Delta E^{\#}$ and $\Delta G^{\#}$ calculated in acetonitrile solution for the different substitutions. In all cases, the values are expressed with respect to the corresponding outer-sphere complex formed between the starting cluster and the entering ligand. The activation barrier calculated for the substitution of Br^- by F^- by an internal associative attack within the outer-sphere complex is moderate, and all of the stationary points in the reaction profile lie below the energy of the starting reactants (Supporting Information), which is in agreement with the experimental observation of a rapid reaction. Because the *b* term in eq 5 can be related to the stability of the outer-sphere complex, the high stability calculated for the case of entering fluoride is also in agreement with the experimental observation of the rate law in eq 5 for the substitutions with this entering anion. In contrast, the values of *b* for other anions would be smaller, and the rate law would be simplified to eq 4.

In the case of chloride as entering ligand, the PES (Figure 10b) reveals two possible pathways with close energy barriers. One of them corresponds to an associative interchange analogous to that described for fluoride as the entering ligand, and the TS (Figure 11b) calculated from the geometry at the MEP in this pathway shows W−Br and W−Cl distances of 3.38 and 2.65 Å, respectively. Although the W−Br distance is now longer, the associative character of the pathway is maintained. In this case, the entering of the chloride is not as clearly assisted by one of the hydrogen atoms of the amino group of the vicinal edpp ligand as in the preceding case because the H−Cl distance is now of 2.10 Å. The other pathway in the PES of Figure 10b corresponds to a dissociative interchange; the transition state (Figure 11c) now shows W−Cl distances of 4.51 and 3.81 Å, respectively. Both distances are much larger than those in the TS for the other

DOI: 10.1021/ic5025313
Inorg. Chem. 2015, 54, 607−618

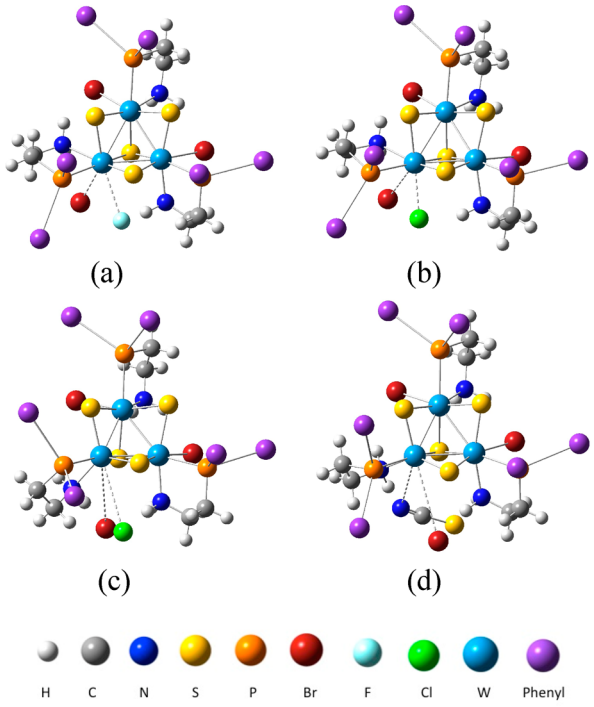

Figure 11. Transition states found for the substitution of the coordinated bromide in $\mathbf{1}^+$. TS for (a) the bromide exchange by fluoride, (b) the associative interchange pathway for the bromide exchange by chloride, (c) the dissociative interchange pathway for the bromide exchange by chloride, and (d) the bromide exchange by thiocyanate. Dashed lines connect the leaving Br and the entering ligand with the metal center. The phenyl groups of the edpp ligands have been substituted by violet spheres for clarity.

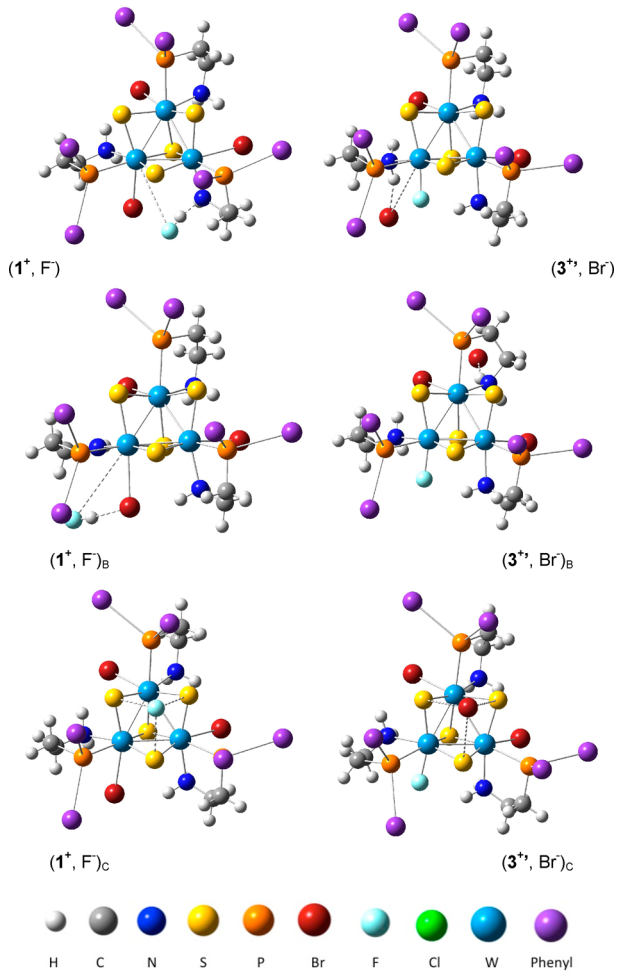

Figure 12. Optimized geometries for the outer-sphere complexes formed by clusters $\mathbf{1}^+$ and $\mathbf{3}^+$ with anions F^- and Br^-, respectively, representing the outer-sphere complexes participating in the substitution of Br^- by F^- through the corresponding pathway in Figure 10a. Dashed lines indicate short contacts and/or long-range interactions. The outer-sphere complexes with subscripts (B or C) correspond to alternative structures that are unproductive in the substitution reaction. The phenyl groups of the edpp ligands have also been omitted for clarity.

pathway so that a partially vacant coordination site can be considered to be generated and the process is accompanied by minor changes in the remaining bond distances. The activation barriers calculated in the gas phase for the two pathways are very close to each other, which suggests that the reaction can go through either of the parallel pathways. However, significant differences are found when the acetonitrile solvent is included in the calculations because the dissociative interchange turns out to be clearly preferred. This can be justified by taking into account that this mechanism implies a greater charge separation than the associative interchange. Thus, it appears that for the bromide-by-chloride exchange both mechanisms are feasible, but the polar acetonitrile solvent would favor the mechanism with a greater charge separation. Unfortunately, the impossibility of obtaining kinetic data for this reaction hinders additional analysis.

For the reaction with thiocyanate (Figure 10c), the calculations were made with the entering ligand coordinating to the metal center through the N atom as found experimentally. In this case, a single pathway is evident in the PES, and optimization of the corresponding transition state (Figure 11d) indicates W–Br and W–N distances of 4.08 and 3.86 Å, respectively. The TS Gibbs free energy is 19 kcal/mol higher than that of the starting reactants (Supporting Information), which is in agreement with the experimental observation of a slower reaction with thiocyanate compared with fluoride. The lower stability of the outer-sphere complex with the entering thiocyanate is also in agreement with the observation of an experimental rate law with the form of eq 4.

In summary, the results of the DFT calculations agree well with the experimental observations, for both the thermodynamic and kinetic aspects. Thus, the energy values in Table 4 agree with the reactivity behavior observed, justifying important observations such as the lack of reactivity of the fluoride-containing cluster with other anions and the order of stability observed ($\mathbf{1}^+ < \mathbf{2}^+ \approx \mathbf{4}^+ < \mathbf{3}^+$). With regard to the kinetics of reaction, the calculated reaction profiles are in all cases compatible with the experimental observation of reactions on the stopped-flow time scale, although with significantly different rate constants. Thus, the reaction of $\mathbf{1}^+$ with F^- is calculated to be faster than with NCS^-, which is in agreement with the experiments. Moreover, the experimental rate laws correlate well with the stabilities calculated for the different outer-sphere complexes so that reactions with fluoride occur with a significant curvature of the kinetic plots (eq 5), whereas other reactions lack this curvature.

CONCLUSIONS

New trinuclear incomplete cubane-type W_3S_4 tungsten clusters bearing aminophosphine ligands have been synthesized for the first time by reacting easily available W_3S_7 precursors with the corresponding ligand. Interestingly, only one of the possible

DOI: 10.1021/ic5025313
Inorg. Chem. 2015, 54, 607–618

Table 5. Summary of the Energies (ΔE, kcal/mol) and the Gibbs Free Energies (ΔG, kcal/mol) Calculated in Acetonitrile Solution for the Formation of the Outer-Sphere Complexes and the Activation Parameters Calculated for the Different Substitution Reactions in Cluster 1^{+a}

outer-sphere complex	ΔE^b	ΔG^b	$\Delta E^{\#\,c}$	$\Delta G^{\#\,c}$
($\mathbf{1}^+$, Cl^-)	−8.8	2.2	17.1[d]	16.5[d]
($\mathbf{1}^+$, F^-)	−27.4	−21.4	16.9	21.3
($\mathbf{1}^+$, NCS^-)	−8.4	2.8	14.8	16.2
($\mathbf{2}^{+\prime}$, Br^-)	−7.3	0.0		
($\mathbf{3}^{+\prime}$, Br^-)	−7.0	−0.9		
($\mathbf{4}^{+\prime}$, Br^-)	−5.9	2.0		
($\mathbf{1}^+$, F^-)$_B$	−25.2	−19.7		
($\mathbf{1}^+$, F^-)$_C$	−16.4	−4.5		
($\mathbf{3}^{+\prime}$, Br^-)$_B$	−6.4	−0.3		
($\mathbf{3}^{+\prime}$, Br^-)$_C$	−3.9	2.5		

[a]Outer-sphere complexes without a subscript are those involved in the substitution reaction, whereas those labeled B and C correspond to alternative structures that are unproductive in the substitution reaction. [b]Relative to the separated ions. [c]Relative to the corresponding outer-sphere complex. [d]These values correspond to the dissociative interchange pathway. The values for the associative interchange pathway are $\Delta E^{\#}$ = 30.3 kcal/mol and $\Delta G^{\#}$ = 28.7 kcal/mol. In the gas phase, the energy differences between both pathways are smaller: $\Delta E^{\#}$ = 27.0 kcal/mol and $\Delta G^{\#}$ = 26.0 kcal/mol for the dissociative interchange and $\Delta E^{\#}$ = 24.3 kcal/mol and $\Delta G^{\#}$ = 25.9 kcal/mol for the associative interchange.

isomers of $[W_3S_4X_3(edpp)_3]^+$ (X = F, Cl, Br, NCS) is formed in almost quantitative yields, and this geometry is maintained in the substitution reactions of the ancillary X^- ligands. In the structure, the nitrogen atoms of the amino group and the terminal halide atoms are located above the trimetallic plane, and the phosphorus atoms are placed below it. These complexes extend the family of phosphine cuboidal W_3S_4 clusters by including an amino group that may have a definite role on catalytic processes.

Substitution of the ancillary X^- ligand occurs readily when thermodynamically favored, and the intermediates involved in the sequential reaction at the three metal centers have been identified by NMR and ESI-MS. However, stopped-flow experiments indicate that these processes occur in a single kinetic step and that the kinetics are controlled by the statistics. In addition, the kinetic data reveal a variety of rate laws for the substitution processes that depend on the nature of the starting cluster and the entering ligand, and the numerical values of the rate constants show differences of several orders of magnitude when varying the entering ligand. The whole set of data can be explained with a mechanism in which there is a rapid pre-equilibrium that leads to the formation of an outer-sphere complex followed by a rate-determining ligand exchange, a process that can show a variety of behaviors according to the results of our DFT calculations. The theoretical work reported herein, including the solvent effects, nicely explains the experimental observations.

Although the limited kinetic data hinders a detailed analysis, it is evident at this time that F^- as the entering ligand leads to very stable outer-sphere complexes (larger K_{os}) because of the interaction with the vicinal amino group, and this interaction assists the substitution process, making it to go faster. However, because the calculations also justify the formation of unproductive outer-sphere complexes with the entering ligand approaching to the cluster far from the entering ligand, there is the possibility of an additional $K'_{os}[Y^-]$ term in the denominator that would contribute to changes in the experimental values of b, thus adding difficulties to the analysis.

In any case, the experimental and theoretical studies described in the present Article provide a detailed kinetic−mechanistic description of substitutions of these clusters in nonaqueous media. Although the lack of protic equilibria simplifies the reaction mechanism with respect to those observed for water substitution by avoiding reaction pathways involving conjugated bases, the mechanistic behavior may be still quite rich because of the possibility of different reaction pathways that differ in the associative/dissociative character of the ligand interchange.

■ ASSOCIATED CONTENT

Supporting Information

CIF and listings of the spectroscopic, spectrometric, and kinetic data for complex salts $\mathbf{1}^+$ to $\mathbf{4}^+$; DFT computed energy profiles; Cartesian coordinates; electronic and Gibbs free energies for the optimized structures; and imaginary frequencies for transition-state structures. This material is available free of charge via the Internet at http://pubs.acs.org.

■ AUTHOR INFORMATION

Corresponding Authors

*E-mail: sixte.safont@qfa.uji.es.
*E-mail: manuel.basallote@uca.es.
*E-mail: rosa.llusar@uji.es.

Author Contributions

[§]T.F.B. and J.A.P.-C.contributed equally to this work.

Notes

The authors declare no competing financial interest.

■ ACKNOWLEDGMENTS

The financial support of the Spanish Ministerio de Economía y Competitividad and FEDER program of the E.U. (grants CTQ2011-23157, CTQ2012-36253-C03-02, and CTQ2012-37821-C02-02), Universitat Jaume I (research project P1·1B2013-19, P1·1B2013-40), Junta de Andalucía (Grupo FQM-137) and Generalitat Valenciana (ACOMP/2013/215 and Prometeo/2014/022) is gratefully acknowledged. We also thank the Servei Central d'Instrumentació Científica (SCIC) of the University Jaume I for providing us with mass spectrometry, NMR, and X-ray facilities. T.F.B. thanks the Spanish Ministerio de Ciencia e Innovación (MICINN) for a doctoral fellowship (FPI). J.A.P.-C. also acknowledges a grant from Junta de Andalucía.

■ DEDICATION

This work is dedicated to the memory of Prof. Zvi Dori.

■ REFERENCES

(1) Zhao, B.; Han, Z.; Ding, K. *Angew. Chem., Int. Ed.* **2013**, *52*, 4744.
(2) Seino, H.; Hidai, M. *Chem. Sci.* **2011**, *2*, 847.
(3) Guillamon, E.; Llusar, R.; Perez-Prieto, J.; Stiriba, S.-E. *J. Organomet. Chem.* **2008**, *693*, 1723.
(4) Algarra, A. G.; Feliz, M.; Fernández-Trujillo, M. J.; Llusar, R.; Safont, V. S.; Vicent, C.; Basallote, M. G. *Chem.—Eur. J.* **2009**, *15*, 4582.
(5) Algarra, A. G.; Basallote, M. G.; Fernández-Trujillo, M. J.; Feliz, M.; Guillamon, E.; Llusar, R.; Sorribes, I.; Vicent, C. *Inorg. Chem.* **2010**, *49*, 5935.
(6) Beltrán, T. F.; Feliz, M.; Llusar, R.; Mata, J. A.; Safont, V. S. *Organometallics* **2011**, *30*, 290.
(7) Beltrán, T. F.; Feliz, M.; Llusar, R.; Safont, V. S.; Vicent, C. *Catal. Today* **2011**, *177*, 72.

DOI: 10.1021/ic5025313
Inorg. Chem. 2015, 54, 607−618

(8) Basallote, M. G.; Fernández-Trujillo, M. J.; Pino-Charnorro, J. A.; Beltrán, T. F.; Corao, C.; Llusar, R.; Sokolov, M.; Vicent, C. *Inorg. Chem.* **2012**, *51*, 6794.
(9) Sorribes, I.; Wienhoefer, G.; Vicent, C.; Junge, K.; Llusar, R.; Beller, M. *Angew. Chem., Int. Ed.* **2012**, *51*, 7794.
(10) Beltrán, T. F.; Feliz, M.; Llusar, R.; Safont, V. S.; Vicent, C. *Eur. J. Inorg. Chem.* **2013**, *2013*, 5797.
(11) Beltrán, T. F.; Llusar, R.; Sokolov, M.; Basallote, M. G.; Fernández-Trujillo, M. J.; Pino-Chamorro, J. A. *Inorg. Chem.* **2013**, *52*, 8713.
(12) Guiry, P. J.; Saunders, C. P. *Adv. Synth. Catal.* **2004**, *346*, 497.
(13) Gopalakrishnan, J. *Appl. Organomet. Chem.* **2009**, *23*, 291.
(14) Stepanova, V. A.; Smoliakova, I. P. *Curr. Org. Chem.* **2012**, *16*, 2893.
(15) Algarra, A. G.; Basallote, M. G.; Feliz, M.; Fernández-Trujillo, M. J.; Guillamon, E.; Llusar, R.; Vicent, C. *Inorg. Chem.* **2006**, *45*, 5576.
(16) Algarra, A. G.; Basallote, M. G.; Feliz, M.; Fernández-Trujillo, M. J.; Llusar, R.; Safont, V. S. *Chem.—Eur. J.* **2006**, *12*, 1413.
(17) Algarra, A. G.; Basallote, M. G.; Feliz, M.; Fernández-Trujillo, M. J.; Llusar, R.; Safont, V. S. *Chem.—Eur. J.* **2010**, *16*, 1613.
(18) Jia, W.; Chen, X.; Guo, R.; Sui-Seng, C.; Amoroso, D.; Lough, A. J.; Abdur-Rashid, K. *Dalton Trans.* **2009**, 8301.
(19) Hounjel, L. J.; Bierenstiel, M.; Ferguson, M. J.; McDonald, R.; Cowie, M. *Inorg. Chem.* **2010**, *49*, 4288.
(20) Xie, J.-B.; Xie, J.-H.; Liu, X.-Y.; Kong, W.-L.; Li, S.; Zhou, Q.-L. *J. Am. Chem. Soc.* **2010**, *132*, 4538.
(21) Xie, J.-B.; Xie, J.-H.; Liu, X.-Y.; Zhang, Q.-Q.; Zhou, Q.-L. *Chem.—Asian J.* **2011**, *6*, 899.
(22) Xie, J.-H.; Liu, X.-Y.; Yang, X.-H.; Xie, J.-B.; Wang, L.-X.; Zhou, Q.-L. *Angew. Chem., Int. Ed.* **2012**, *51*, 201.
(23) Zhu, S.-F.; Yu, Y.-B.; Li, S.; Wang, L.-X.; Zhou, Q.-L. *Angew. Chem., Int. Ed.* **2012**, *51*, 8872.
(24) Fuentes, J. A.; Carpenter, I.; Kann, N.; Clarke, M. L. *Chem. Commun.* **2013**, *49*, 10245.
(25) Kayan, C.; Meric, N.; Aydemir, M.; Ocak, Y. S.; Baysal, A.; Temel, H. *Appl. Organomet. Chem.* **2014**, *28*, 127.
(26) Rafikova, K.; Kystaubayeva, N.; Aydemir, M.; Kayan, C.; Ocak, Y. S.; Temel, H.; Zazybin, A.; Gurbuz, N.; Ozdemir, I. *J. Organomet. Chem.* **2014**, *758*, 1.
(27) Estevan, F.; Feliz, M.; Llusar, R.; Mata, J. A.; Uriel, S. *Polyhedron* **2001**, *20*, 527.
(28) Feliz, M.; Guillamon, E.; Llusar, R.; Vicent, C.; Stiriba, S. E.; Perez-Prieto, J.; Barberis, M. *Chem.—Eur. J.* **2006**, *12*, 1486.
(29) Llusar, R.; Vicent, C. In *Inorganic Chemistry in Focus III*; Meyer, G., Naumann, D., Wesermann, L., Eds.; Wiley: Weinheim, Germany, 2006; pp 105−121.
(30) Algarra, A. G.; Basallote, M. G.; Fernández-Trujillo, M. J.; Guillamon, E.; Llusar, R.; Segarra, M. D.; Vicent, C. *Inorg. Chem.* **2007**, *46*, 7668.
(31) Ooi, B. L.; Sykes, A. G. *Inorg. Chem.* **1988**, *27*, 310.
(32) Ooi, B. L.; Sykes, A. G. *Inorg. Chem.* **1989**, *28*, 3799.
(33) Hernández-Molina, R.; Sykes, A. G. *Coord. Chem. Rev.* **1999**, *187*, 291.
(34) Hernández-Molina, R.; Sykes, A. G. *J. Chem. Soc., Dalton Trans.* **1999**, 3137.
(35) Hernández-Molina, R.; Sokolov, M. N.; Sykes, A. G. *Acc. Chem. Res.* **2001**, *34*, 223.
(36) *MassLynx*, 4.0 ed.; Itd, W., Ed.; Waters: Milford, MA, 2005.
(37) Fedin, V. P.; Sokolov, M. N.; Gerasko, O. A.; Kolesov, B. A.; Fedorov, V. Y.; Mironov, A. V.; Yufit, D. S.; Slovohotov, Y. L.; Struchkov, Y. T. *Inorg. Chim. Acta* **1990**, *175*, 217.
(38) *CrysAlisPro*, version 171.36.24; Agilent Technologies: Santa Clara, CA, 2012.
(39) Clark, R. C.; Reid, J. S. *Acta Crystallogr., Sect. A* **1995**, *51*, 887.
(40) Sheldrick, G. M. *Acta Crystallogr., Sect. A* **2008**, *64*, 112.
(41) Dolomanov, O. V.; Bourhis, L. J.; Gildea, R. J.; Howard, J. A. K.; Puschmann, H. *J. Appl. Crystallogr.* **2009**, *42*, 339.
(42) Brandenburg, K.; Putz, H. *Diamond: Crystal and Molecular Structure Visualization*; Crystal Impact: Bonn, Germany, 2008. http://www.crystalimpact.com/diamond
(43) Binstead, R. A.; Jung, B.; Zuberbühler, A. D.; *SPECFIT/32*; Spectrum Software Associates: Chapel Hill, NC, 2000.
(44) Lee, C. T.; Yang, W. T.; Parr, R. G. *Phys. Rev. B* **1988**, *37*, 785.
(45) Frisch, M. J.; Trucks, G. W.; Schlegel, H. B.; Scuseria, G. E.; Robb, M. A.; Cheeseman, J. R.; Scalmani, G.; Barone, V.; Mennucci, B.; Petersson, G. A.; Nakatsuji, H.; Caricato, M.; Li, X.; Hratchian, H. P.; Izmaylov, A. F.; Bloino, J.; Zheng, G.; Sonnenberg, J. L.; Hada, M.; Ehara, M.; Toyota, K.; Fukuda, R.; Hasegawa, J.; Ishida, M.; Nakajima, T.; Honda, Y.; Kitao, O.; Nakai, H.; Vreven, T.; Montgomery, J. A., Jr.; Peralta, J. E.; Ogliaro, F.; Bearpark, M.; Heyd, J. J.; Brothers, E.; Kudin, K. N.; Staroverov, V. N.; Kobayashi, R.; Normand, J.; Raghavachari, K.; Rendell, A.; Burant, J. C.; Iyengar, S. S.; Tomasi, J.; Cossi, M.; Rega, N.; Millam, N. J.; Klene, M.; Knox, J. E.; Cross, J. B.; Bakken, V.; Adamo, C.; Jaramillo, J.; Gomperts, R.; Stratmann, R. E.; Yazyev, O.; Austin, A. J.; Cammi, R.; Pomelli, C.; Ochterski, J. W.; Martin, R. L.; Morokuma, K.; Zakrzewski, V. G.; Voth, G. A.; Salvador, P.; Dannenberg, J. J.; Dapprich, S.; Daniels, A. D.; Farkas, Ö.; Foresman, J. B.; Ortiz, J. V.; Cioslowski, J.; Fox, D. J. *Gaussian 09*, revision D.01; Gaussian, Inc.: Wallingford, CT, 2009.
(46) Feliz, M.; Llusar, R.; Andres, J.; Berski, S.; Silvi, B. *New J. Chem.* **2002**, *26*, 844.
(47) Vicent, C.; Feliz, M.; Llusar, R. *J. Phys. Chem. A* **2008**, *112*, 12550.
(48) Fukui, K. *Acc. Chem. Res.* **1981**, *14*, 363.
(49) Miertus, S.; Scrocco, E.; Tomasi, J. *Chem. Phys.* **1981**, *55*, 117.
(50) Pascual-Ahuir, J. L.; Silla, E.; Tunon, I. *J. Comput. Chem.* **1994**, *15*, 1127.
(51) Cotton, F. A.; Llusar, R. *Polyhedron* **1987**, *6*, 1741.
(52) Sasaki, M.; Sakane, G.; Ouchi, T.; Shibahara, T. *J. Cluster Sci.* **1998**, *9*, 25.
(53) Beltrán, T. F. *Clústeres Sulfuro Trimetálicos de Molibdeno y Wolframio Funcionalizados con Ligandos Difosfina o Aminofosfina y sus Aplicaciones en Catálisis Orgánica*. Ph. D. Thesis, Universitat Jaume I, Castellón de la Plana, Spain, September 2013. ISBN: 978-84-697-1305-1.
(54) Ball, N. D.; Kampf, J. W.; Sanford, M. S. *Dalton Trans.* **2010**, *39*, 632.
(55) Algarra, A. G.; Fernández-Trujillo, M. J.; Basallote, M. G. *Chem.—Eur. J.* **2012**, *18*, 5036.
(56) Algarra, A. S. G.; Basallote, M. G.; Fernández-Trujillo, M. J.; Llusar, R.; Safont, V. S.; Vicent, C. *Inorg. Chem.* **2006**, *45*, 5774.

DOI: 10.1021/ic5025313
Inorg. Chem. 2015, 54, 607−618